Supplementary material for: Evaluating the carbon and nitrogen cycles of the QUINCY terrestrial biosphere model using remotely-sensed data

Tuuli Miinalainen[1,2,3], Amanda Ojasalo[1,4], Sönke Zaehle[3], Holly Croft[5], Mika Aurela[2], Mikko Peltoniemi[6], Silvia Caldararu[7], and Tea Thum[2]

[1]Earth Observation Research, Finnish Meteorological Institute, P.O. Box 503, 00101 Helsinki, Finland
[2]Climate System Research, Finnish Meteorological Institute, P.O. Box 503, 00101 Helsinki, Finland
[3]Department of Biogeochemical Signals, Max Planck Institute for Biogeochemistry, Hans-Knöll-Straße 10, 07745 Jena, Germany
[4]Department of Geosciences and Geography, University of Helsinki, Gustaf Hällströmin katu 2, 00560 Helsinki, Finland
[5]School of Biosciences, University of Sheffield, Western Bank, Sheffield, S10 2TN, United Kingdom
[6]Natural Resources Institute Finland, Helsinki, Finland
[7]Discipline of Botany, School of Natural Sciences, Trinity College Dublin, College Green, Dublin 2, Ireland

Table S1. A list of QUINCY simulations

Name	Description	Sites
QUINCY default	default parametrization	PLUMBER2 & GLOBAL
QUINCY C_{only}	default parametrization, but C-cycle only enabled and with a fixed leaf stoichiometry	PLUMBER2
QUINCY $f_{N,chl}$ increase	Same as QUINCY default, but $f_{N,chl}$ increased by 30 %	PLUMBER2, only TeBS
QUINCY alter N frac	Same as QUINCY default, but leaf N allocation with the alternative scheme (see Section 2.1.2)	PLUMBER2
QUINCY alter N frac, $f_{N,rub}$ increase	Same as QUINCY alter N frac, but $f_{N,rub}$ increased by 30 %	PLUMBER2, only TeBS

Table S2. Lanc cover (LC) classes used in the RS chl_{leaf} postprocessing. Based on ESA-CCI-LC documentation (ESA, 2017).

LC value	LC description	LC value	LC description
10	Cropland, rainfed	81	Tree cover, needle-leaved, deciduous, closed (>40%)
11	Herbaceous cover	82	Tree cover, needle-leaved, deciduous, open (15-40%)
20	Cropland, irrigated or post-flooding	90	Tree cover, mixed leaf type (broad-leaved and needle-leaved)
30	Mosaic cropland (>50%) / natural vegetation (tree, shrub, herbaceous cover) (<50%)	110	Mosaic herbaceous cover (>50%) /tree and shrub (<50%)
40	Mosaic natural vegetation (tree, shrub, herbaceous cover/ (>50%) / cropland (<50%)	120	Shrubland
50	Tree cover, broad-leaved, evergreen, closed to open	121	Evergreen shrubland
60	Tree cover, broad-leaved, deciduous, closed to open	122	Deciduous shrubland
61	Tree cover, broad-leaved, deciduous, closed	130	Grassland
62	Tree cover, broad-leaved, deciduous, open	140	Lichens and mosses
70	Tree cover, needle-leaved, evergreen, closed to open	150	Sparse vegetation (tree, shrub, herbaceous cover) (< 15%)
71	Tree cover, needle-leaved, evergreen, closed (>40%)	160	Tree cover, flooded, fresh or brakish water
72	Tree cover, needle-leaved, evergreen, open (15-40%)	180	Shrub or herbaveous cover, flooded, fresh/saline/brakish water
80	Tree cover, needle-leaved, deciduous, closed to open (>15%)		

Table S3. QUINCY plant functional types and the corresponding land cover (LC) types. The LC classes are listed in Table S2

Abbreviation	Long name	LC classes
BNE	Boreal needle-leaved evergreen	70, 71, 72, 90, 160
TeNE	Temperate needle-leaved evergreen	70, 71, 72, 90, 160
BNS	Boreal needle-leaved deciduous	80, 81, 82, 90, 160
TeBE	Temperate broad-leaved evergreen	40, 50, 90, 160
TeBS	Temperate broad-leaved deciduous	40, 60, 61, 62, 90, 160
TrBR	Tropical broad-leaved rain deciduous	60, 61, 62, 90, 160
TrBE	Tropical broad-leaved evergreen	50, 90, 160
TeC	C3 crops	10, 11, 20, 30, 110, 120, 121, 122, 130, 140, 150, 180
TeH	C3 grasslands	10, 11, 20, 30, 110, 120, 121, 122, 130, 140, 150, 180
TrH	C4 grasslands	10, 11, 20, 30, 110, 120, 121, 122, 130, 140, 150

Table S4. PFT means of chl_{leaf}, the 90th percentile of LAI, and GPP annual sums for the PLUMBER2 sites for QUINCY, remote sensing (RS), and flux tower observations of GPP. The numbers indicate the mean value of the site-level mean chl_{leaf} $\pm$ the standard deviation. Values are calculated based on site-level mean chl_{leaf} and GPP mean annual sum. Statistically significant ($p < 0.05$) correlation coefficients are marked with an asterisk. The PFT abbreviations are defined in Table 1.

PFT	chl_{leaf} ($\mu g\,cm^{-2}$)			LAI ($m^2\,m^{-2}$)			GPP ($gCm^{-2}yr^{-1}$)		
	QUINCY	RS	r	QUINCY	RS	r	QUINCY	Observations	r
BNE	44.4±9.4	41.3±25.4	0.66*	3.7±1.0	3.5±1.1	0.80*	935±365	1235±556	0.80*
TeNE	59.9±8.9	48.3±12.9	0.01	4.5±0.4	3.0±1.1	-0.48	1713±377	1805±241	0.30
TeBE	40.5±5.8	20.4±5.4	0.85	4.8±0.3	3.0±1.4	0.88	1970±350	1698±369	-0.37
TeBS	17.9±5.6	22.1±6.1	0.71*	4.1±0.6	4.4±1.5	0.42*	1232±367	1539±377	0.25
TrBR	26.4±13.7	10.2±0.0	-	4.6±1.2	1.9±1.1	-	1820±1018	1488±483	-
TrBE	45.7±9.0	55.8±13.2	0.22	4.7±0.2	4.5±1.3	0.42	2401±607	2445±872	0.64
TeC	13.7±1.4	28.4±10.4	0.11	4.5±1.8	3.3±1.2	-0.03	1437±469	1228±303	0.13
TeH	12.0±2.6	21.1±11.9	-0.04	3.1±1.9	2.6±1.5	0.55*	1004±545	977±687	0.77*
TrH	45.3±5.3	38.3±11.3	0.16	2.1±1.3	1.6±1.1	0.59*	756±416	902±502	0.52*
all	28.3±17.4	31.1±17.4	0.61*	3.7±1.6	3.1±1.6	0.51*	1229±620	1304±658	0.71*

Table S5. Group-based PFT means of chl_{leaf} and LAI 90th percentile time series for the PLUMBER2 and GLOBAL sites. The numbers indicate the mean value $\pm$ the standard deviation, and the minimum and maximum values are in parentheses. The values are calculated based on the site-level mean chl_{leaf} and LAI 90th percentile.

PFT	chl_{leaf} ($\mu g\,cm^{-2}$		LAI ($m^2\,m^{-2}$)	
	QUINCY	Remote sensing	QUINCY	Remote sensing
BNE	39.0±7.0 (32.0–62.4)	33.1±17.9 (6.3–95.0)	3.1±1.1 (1.4–5.2)	3.5±1.0 (1.0–5.9)
TeNE	63.1±8.5 (38.9–71.9)	44.5±12.6 (20.5–74.5)	4.7±0.4 (3.7–5.0)	3.5±1.3 (0.4–5.6)
BNS	11.8±1.1 (10.5–12.9)	10.7±7.2 (4.0–20.4)	1.2±0.5 (0.5–1.7)	3.0±0.9 (2.1–4.4)
TeBE	42.3±5.4 (35.6–49.5)	22.7±8.6 (13.0–37.0)	4.9±0.4 (4.3–5.4)	3.3±1.2 (1.4–4.6)
TeBS	16.2±6.4 (5.3–32.8)	20.1±6.7 (6.7–35.5)	4.1±0.7 (1.0–5.0)	4.4±1.3 (1.2–6.3)
TrBR	20.6±10.4 (13.8–36.1)	13.2±3.5 (10.2–16.8)	4.1±0.9 (3.4–5.4)	2.7±1.1 (1.1–3.8)
TrBE	46.8±5.0 (33.0–59.7)	57.3±11.9 (26.4–78.7)	5.0±0.3 (4.2–5.5)	5.0±1.0 (2.0–6.1)
TeC	13.7±1.4 (10.5–16.7)	28.4±10.4 (13.2–46.3)	4.5±1.8 (1.9–7.3)	3.3±1.2 (1.5–5.2)
TeH	10.0±3.1 (4.6–17.2)	21.9±11.0 (2.0–47.1)	2.4±1.5 (0.4–7.9)	1.9±1.4 (0.2–5.5)
TrH	49.3±8.6 (31.9–71.8)	38.7±10.3 (12.2–62.4)	4.3±3.1 (0.6–12.2)	1.8±1.3 (0.1–5.4)
all	31.9±18.7 (4.6–71.9)	32.5±16.7 (2.0–95.0)	3.7±2.1 (0.4–12.2)	2.9±1.7 (0.1–6.3)

Table S6. The annual average $\mathrm{chl}_{\mathrm{leaf}} \pm$ std values and annual GPP sum for FI-Sod and US-NR1. DJF (December–February) and JJA (June–August) mean values are also listed. The numerical ranges are shown in parentheses after the annual means.

Sodankylä (FI-Sod)					
Variable	Season	QUINCY	RS, Croft et al. (2020)	RS, Sentinel-3	In-situ
$\mathrm{chl}_{\mathrm{leaf}}$ ($\mu\mathrm{g\,cm^{-2}}$)	yearly mean	35.0±1.2 (33–39)	18.4±4.7 (8–32)	16.1±9.3 (0–51)	57.9±10.4 (40–78)
$\mathrm{chl}_{\mathrm{leaf}}$ ($\mu\mathrm{g\,cm^{-2}}$)	DJF	33.9±0.3	18.2±3.8	-	-
$\mathrm{chl}_{\mathrm{leaf}}$($\mu\mathrm{g\,cm^{-2}}$)	JJA	36.1±0.6	20.1±5.0	21.1±6.8	62.6±7.8
GPP ($\mathrm{gC\,m^{-2}\,yr^{-1}}$)	annual sum	545±52	-	-	602±82
Niwot-Ridge (US-NR1)					
Variable	Season	QUINCY	RS, Croft et al. (2020)	RS, Sentinel-3	In-situ
$\mathrm{chl}_{\mathrm{leaf}}$ ($\mu\mathrm{g\,cm^{-2}}$)	yearly mean	34.8±0.8 (33–38)	25.3±6.3 (7-–52)	33.2±12.4 (3—55)	40.5±5.1 (27—46)
$\mathrm{chl}_{\mathrm{leaf}}$ ($\mu\mathrm{g\,cm^{-2}}$)	DJF	34.0±0.3	25.5±2.9	21.2±9.3	-
$\mathrm{chl}_{\mathrm{leaf}}$ ($\mu\mathrm{g\,cm^{-2}}$)	JJA	35.5±0.6	24.3±8.9	46.7±4.8	43.2±2.3
GPP ($\mathrm{gC\,m^{-2}\,yr^{-1}}$)	annual sum	467±34	-	-	845±44

Table S7. PFT mean values for the mean chl_{leaf}, LAI 90th percentile and annual GPP for the PLUMBER2 sites with default QUINCY ("Q def.", QUINCY with alternative N fraction scheme ("Q alter N") and remote sensing (RS) and eddy flux covariance observations. $f_{N,struct}$ values are calculated as average JJA (June-August) fractions.

PFT	nr sites	$f_{N,struct}$ (-)		chl_{leaf} ($\mu g\,cm^{-2}$)			LAI ($m^2\,m^{-2}$)			GPP ($gC\,m^{-2}\,yr^{-1}$)		
		Q def.	Q alter N	Q def.	Q alter N	RS	Q def.	Q alter N	RS	Q def.	Q alter N	Obs
BNE	20	0.66	0.86	44.4±9.4	16.4±3.2	41.3±25.4	3.7±1.0	3.2±0.9	3.5±1.1	935±365	716±295	1235±556
TeNE	8	0.66	0.86	59.9±8.9	20.6±2.7	48.3±12.9	4.5±0.4	4.1±0.4	3.1±1.2	1713±377	1418±331	1805±241
TeBE	4	0.53	0.77	40.5±5.8	22.1±1.7	20.4±5.4	4.8±0.3	4.2±0.3	3.1±1.4	1970±350	1468±236	1698±369
TeBS	25	0.51	0.69	17.9±5.6	14.9±4.4	22.1±6.1	4.1±0.6	3.8±0.5	4.5±1.5	1231±366	1044±311	1539±377
TrBR	2	0.52	0.69	26.4±13.7	21.7±11.9	10.2±0.0	4.6±1.2	4.1±1.3	1.9±1.1	1820±1019	1553±977	1488±483
TrBE	9	0.58	0.76	45.7±9.0	26.6±4.7	55.8±13.2	4.8±0.2	4.5±0.2	4.6±1.3	2401±607	2125±585	2445±872
TeC	11	0.23	0.65	14.2±1.3	12.1±0.9	31.6±10.3	5.3±2.1	3.2±0.6	2.9±1.0	1569±505	790±171	1329±261
TeH	13	0.25	0.65	12.7±2.5	11.1±1.6	28.6±11.0	3.1±2.1	2.1±1.1	2.1±1.4	972±603	531 ±319	774±619
TrH	20	0.3	0.42	45.3±5.3	25.7±4.4	38.3±11.3	2.2±1.4	2.6±1.8	1.6±1.1	756±416	974±596	902±502
all	112	0.46	0.69	32.8±17.2	18.1±6.5	34.4±17.5	3.8±1.6	3.3±1.2	3.2±1.6	1262 ±648	1026 ±570	1358 ±664

Table S8. The mean chl_{leaf}, mean 90th percentile of LAI and annual GPP for the PLUMBER2 temperate broad-leaved deciduous (TeBS) sites for different QUINCY simulations ± standard deviation between sites.

	chl_{leaf} ($\mu g\,cm^{-2}$)	LAI ($m^2\,m^{-2}$)	GPP ($gC\,m^{-2}\,yr^{-1}$)
QUINCY default	17.9±5.6	4.1±0.6	1231±366
QUINCY default, 1.3x $f_{N,chl}$	24.6±7.6	4.0±0.5	1153±338
QUINCY alter N frac	14.9±4.4	3.8±0.5	1044±311
QUINCY alter N frac, 1.3x $f_{N,rub}$	18.5±5.7	4.0±0.5	1170±337
observations	22.1±6.1	4.5±1.5	1539±377

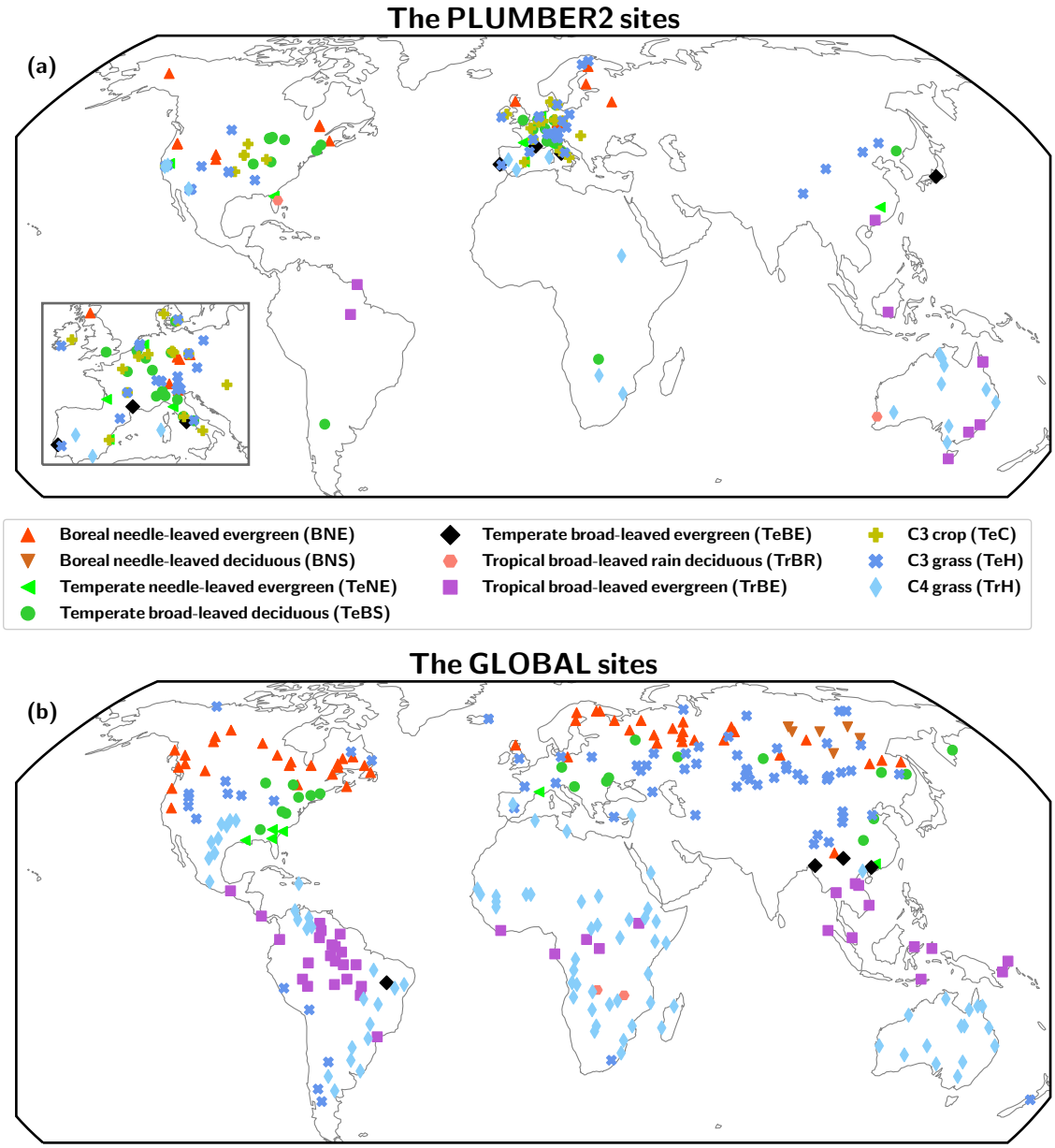

Figure S1. A map of the **(a)** PLUMBER2 sites and of the **(b)** GLOBAL sites. Different colors and markers indicate the PFT. A separate map of Europe is inserted in **(a)**.

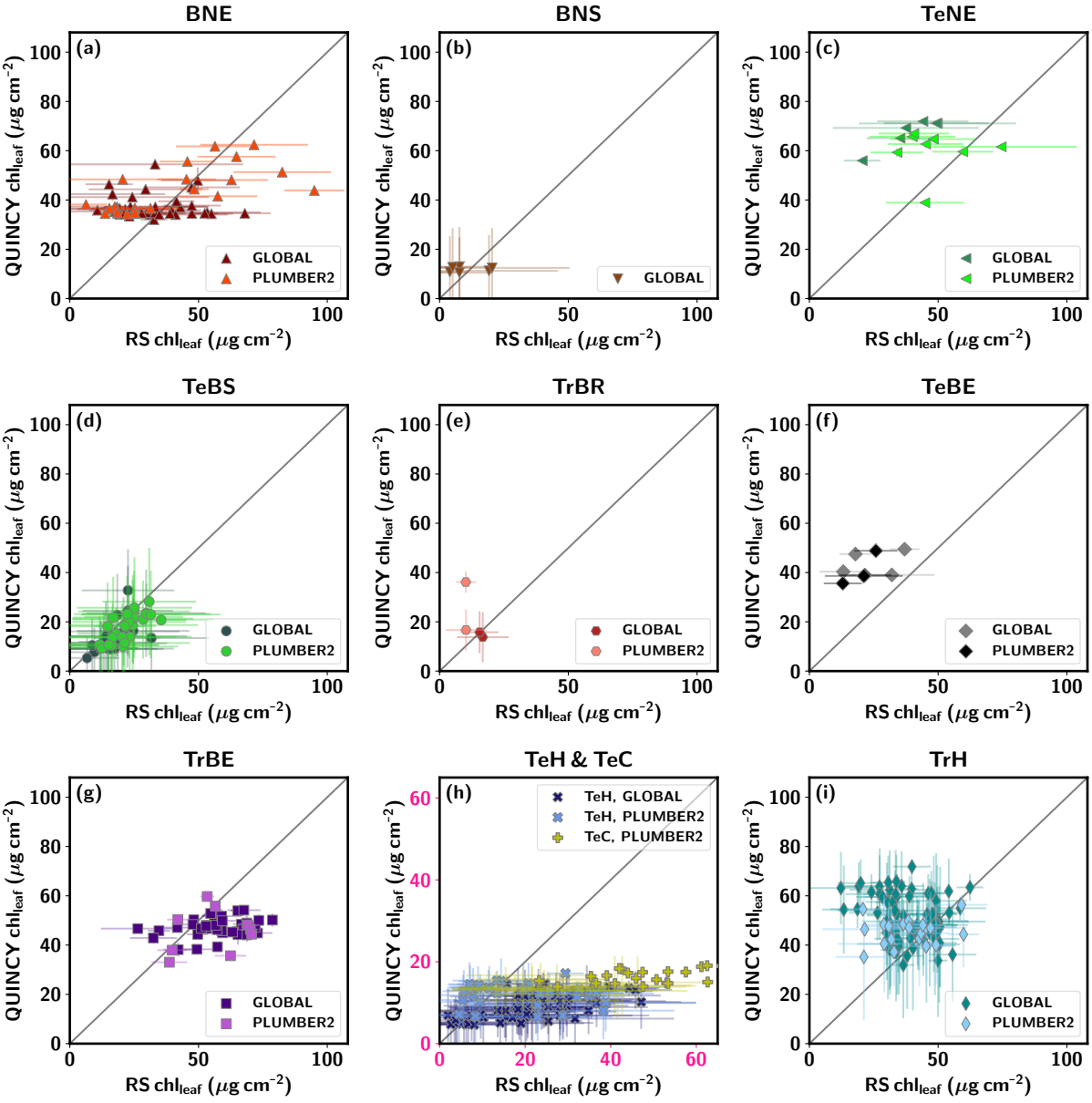

Figure S2. The mean site-level chl_{leaf} for the PLUMBER2 and GLOBAL sites for RS and QUINCY. Each marker represents one site. The whiskers show the mean interannual standard deviation for each site. Subplot **(h)** has a different scale on the x- and y-axis than the other subplots.

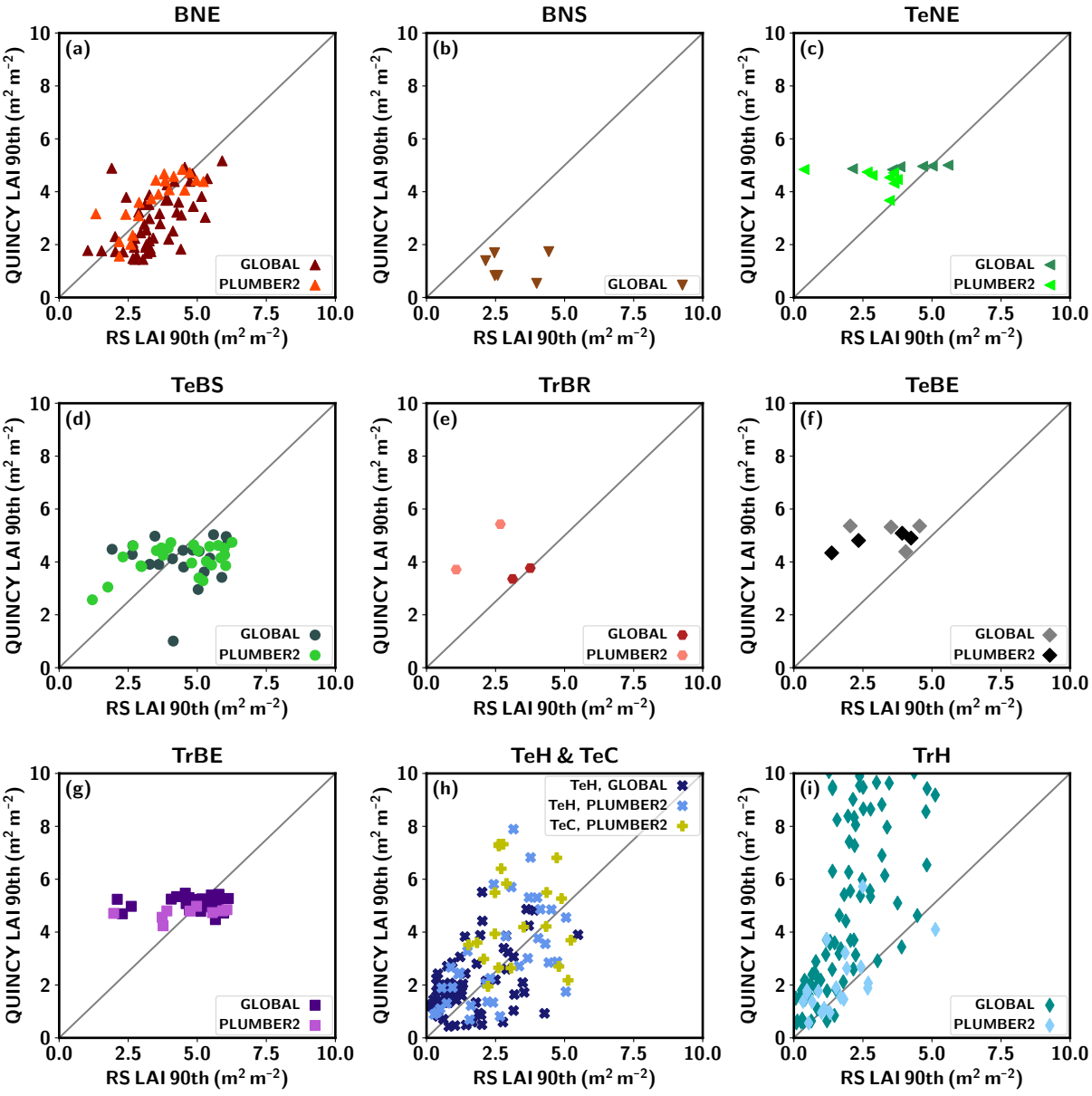

Figure S3. The site-level 90th percentiles of LAI for the PLUMBER2 and GLOBAL sites for RS and QUINCY.

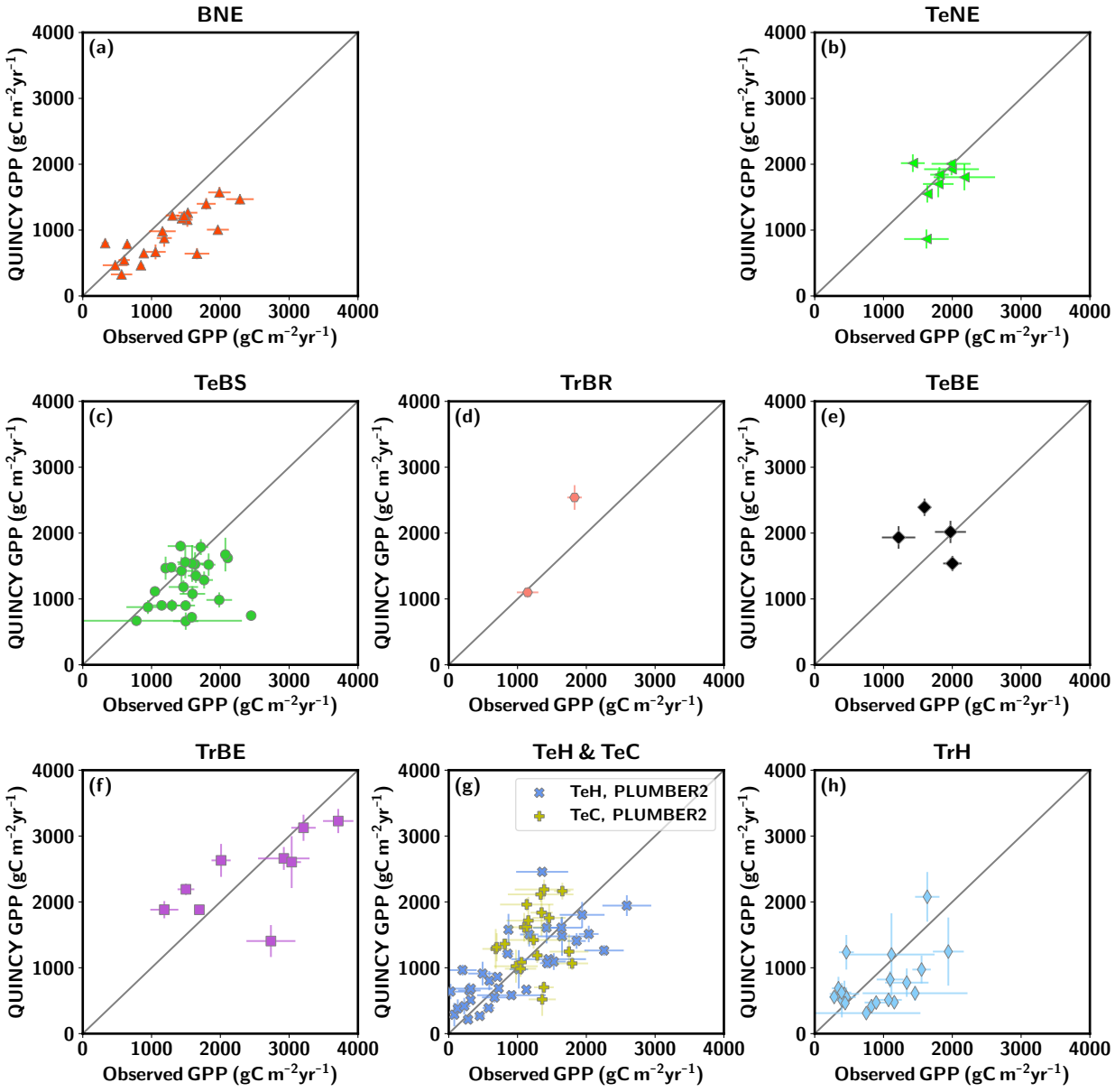

Figure S4. The mean annual GPP for different sites from the PLUMBER2 sites. The whiskers indicate the standard deviation calculated between annual GPP for different years. In the PLUMBER2 site set, there were no GPP ground observations for the boreal needle-leaved deciduous (BNS) PFT.

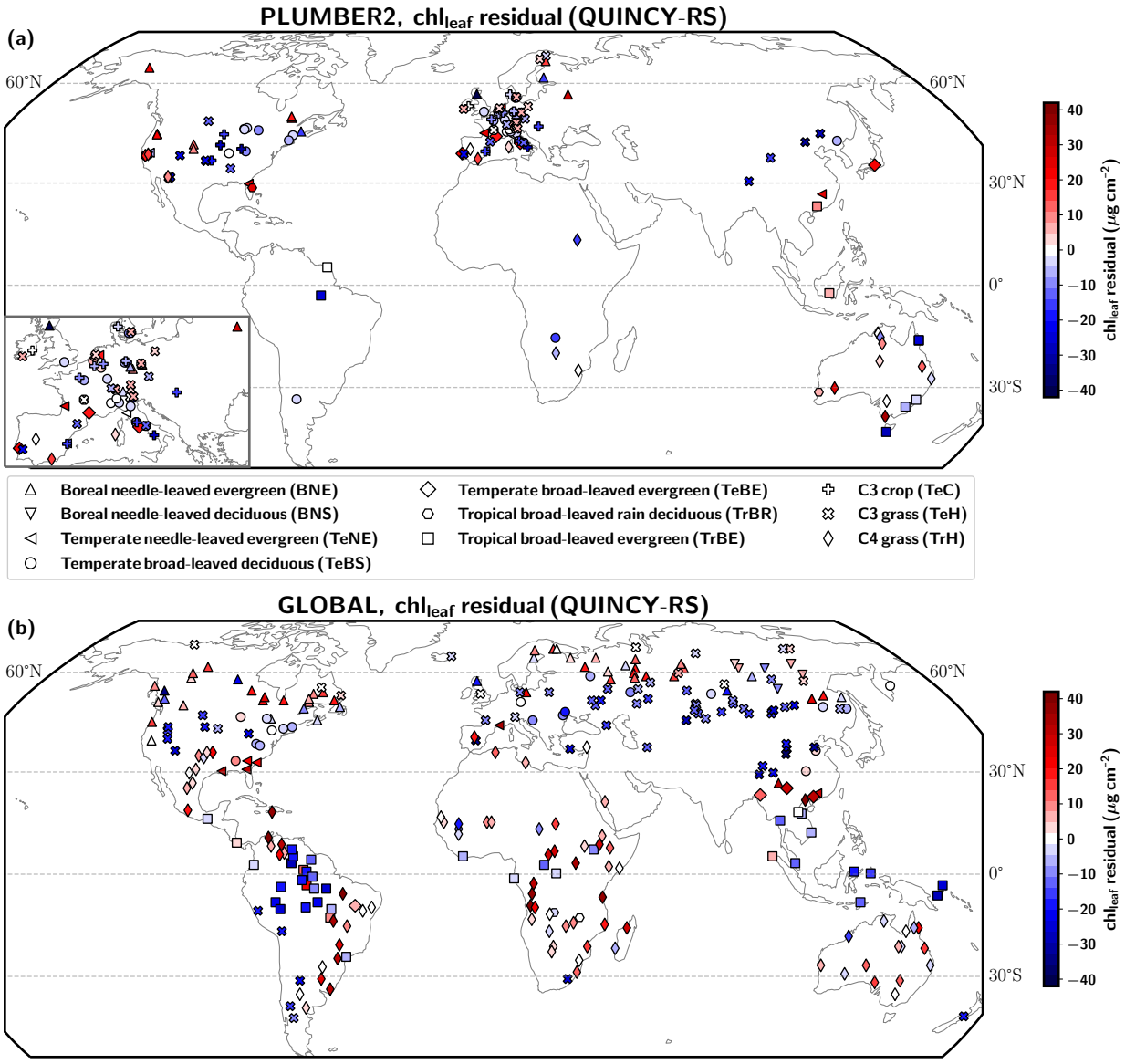

Figure S5. The residual chl_{leaf} between the mean values of QUINCY and RS for **(a)** PLUMBER2 and **(b)** GLOBAL sites. Each marker represents one site.

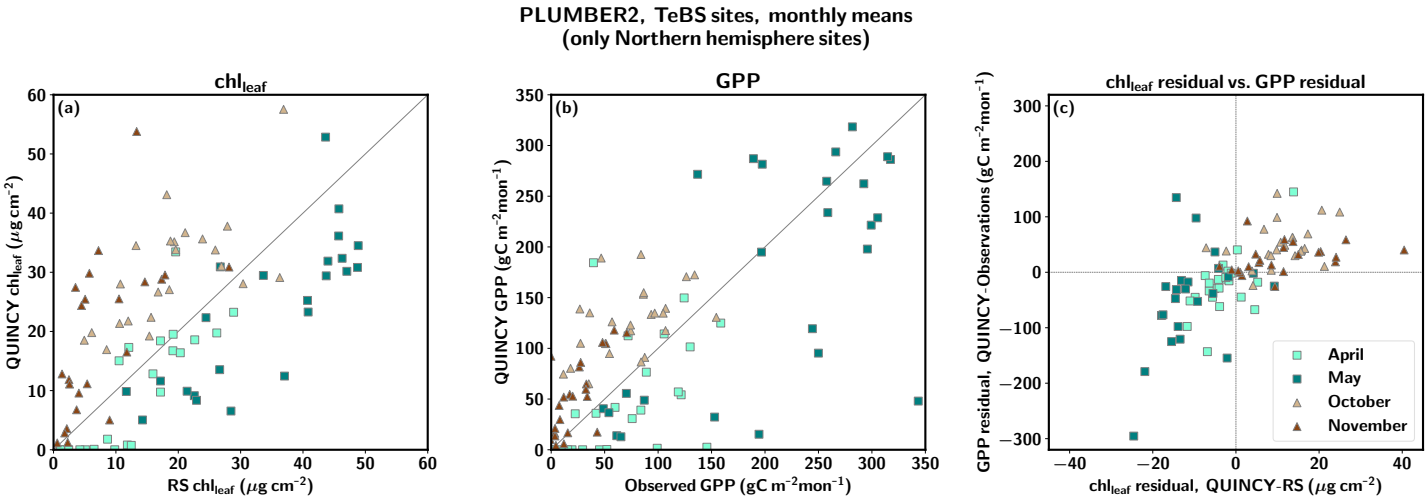

Figure S6. Averaged monthly values for April (cyan), May (turquoise), October (beige), and November (brown) for the PLUMBER2 Northern Hemisphere sites. **(a)** Mean $\mathrm{chl}_{\mathrm{leaf}}$, **(b)** GPP sum, and **(c)** $\mathrm{chl}_{\mathrm{leaf}}$ residual and GPP residual. Residuals are calculated between mean QUINCY and observations. Each marker represents one site.

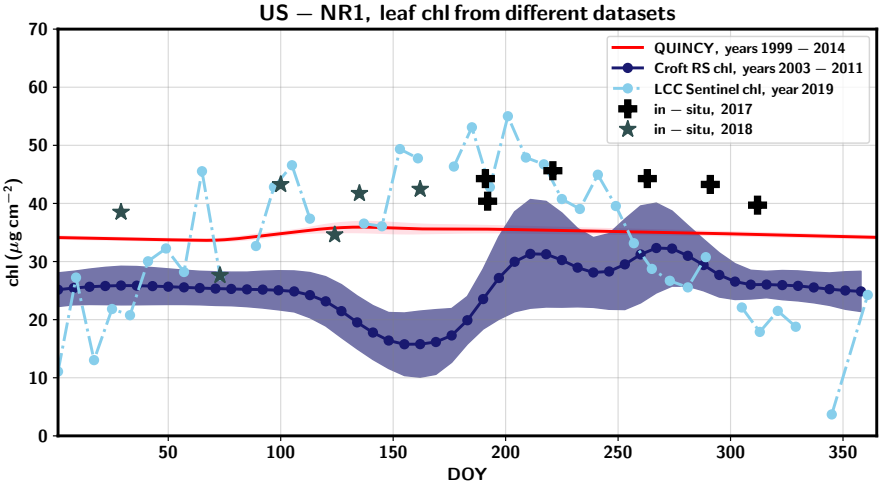

Figure S7. Seasonal cycle of daily averages for US-NR1 for $\mathrm{chl}_{\mathrm{leaf}}$.

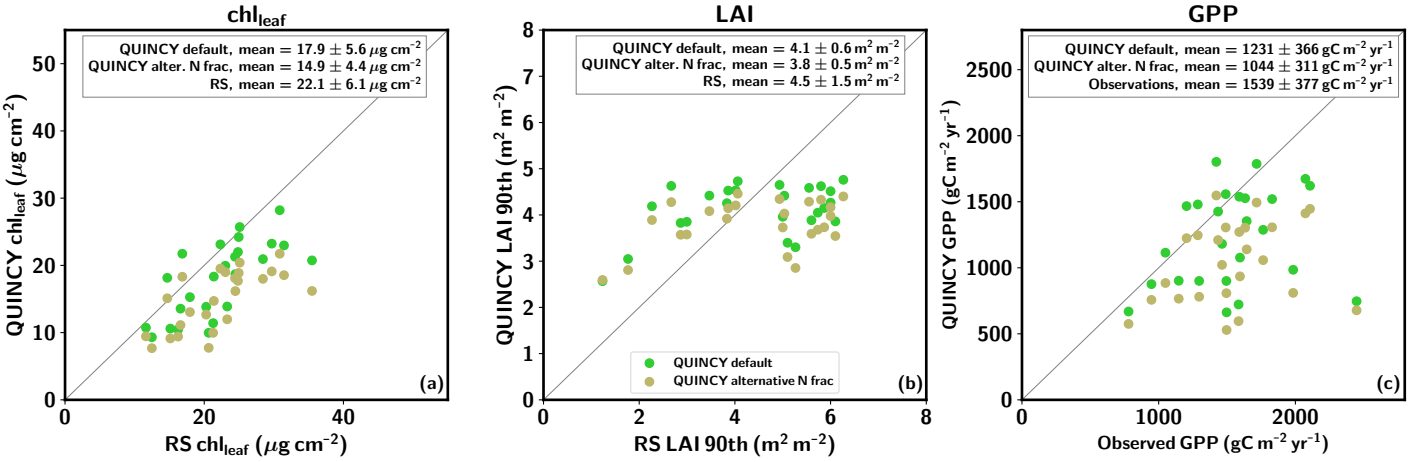

Figure S8. **(a)** The mean $\mathrm{chl}_{\mathrm{leaf}}$, **(b)** mean annual 90th percentile of LAI, and **(c)** annual GPP for the TeBS PLUMBER2 sites for QUINCY default and QUINCY alternative N fraction simulations and observations.

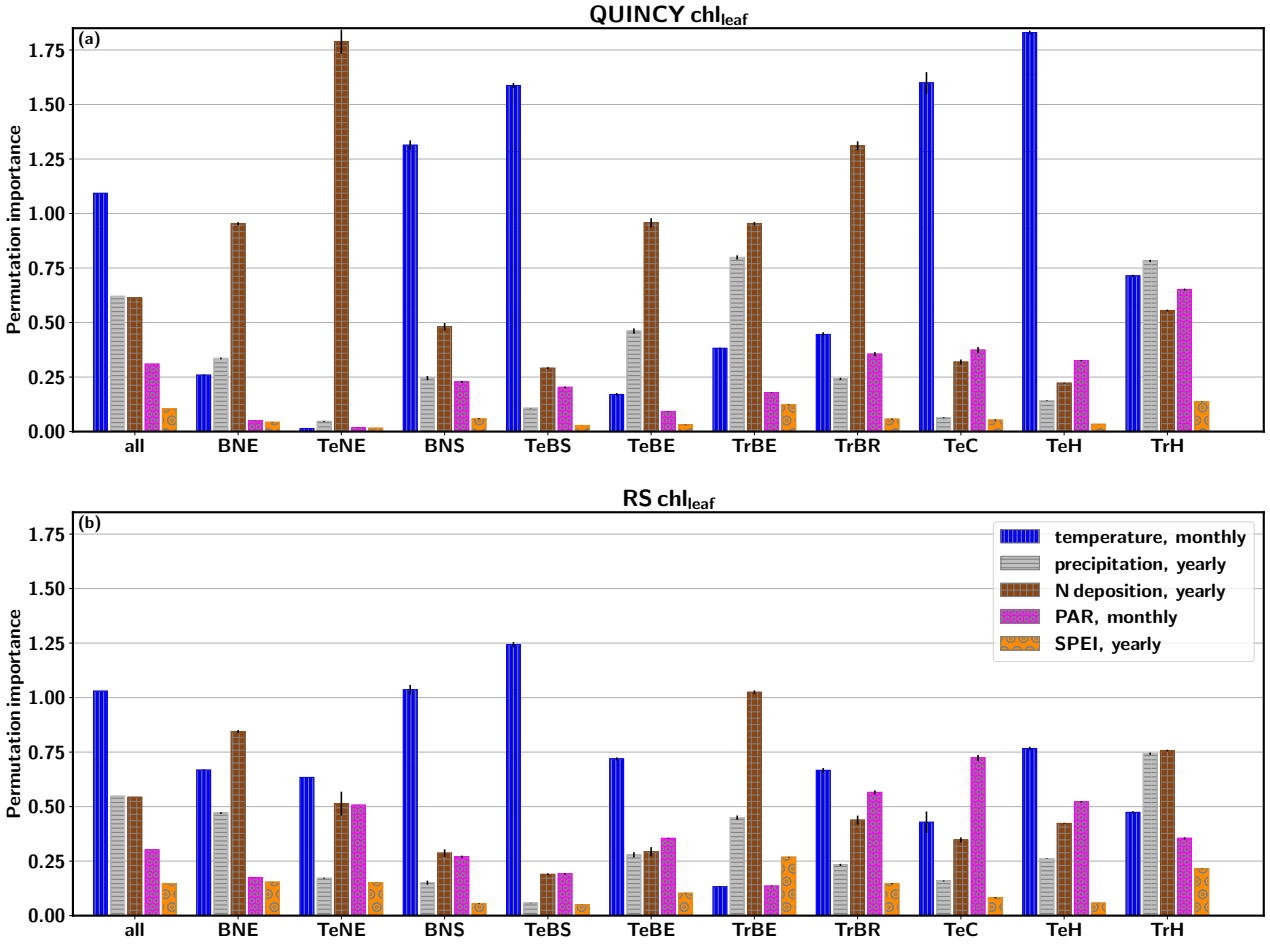

Figure S9. The permutation importance values for different PFTs after random forest regression fitting for **(a)** QUINCY $\mathrm{chl}_{\mathrm{leaf}}$ and **(b)** RS $\mathrm{chl}_{\mathrm{leaf}}$.

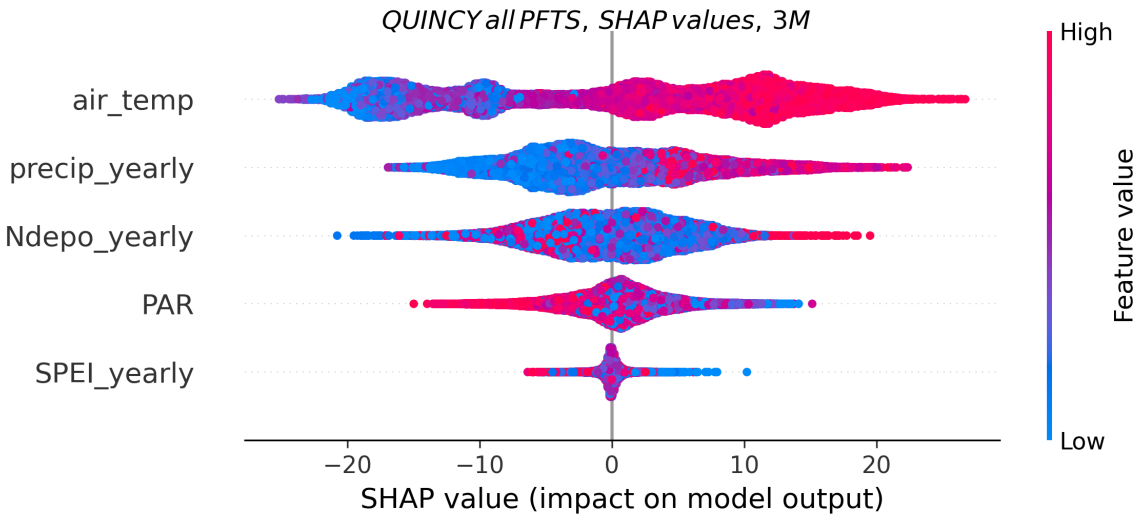

Figure S10. SHAP values of the random forest regression fit for the QUINCY chl_{leaf}, using three-month and annual averages. Each point represents a three-month average, and the color indicates the feature value. The more blue values correspond to low feature values, and the more red values correspond to high feature values.

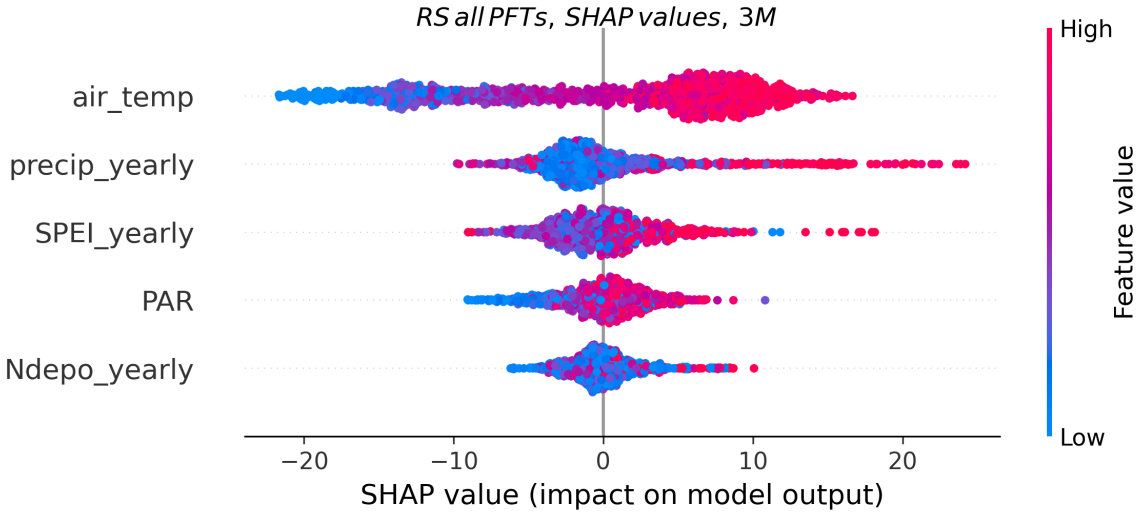

Figure S11. SHAP values of the random forest regression fit for the RS chl_{leaf}, using three-month and annual averages.

References

Croft, H., Chen, J., Wang, R., Mo, G., Luo, S., Luo, X., He, L., Gonsamo, A., Arabian, J., Zhang, Y., Simic-Milas, A., Noland, T., He, Y., Homolová, L., Malenovský, Z., Yi, Q., Beringer, J., Amiri, R., Hutley, L., Arellano, P., Stahl, C., and Bonal, D.: The global distribution of leaf chlorophyll content, Remote Sensing of Environment, 236, 111 479, https://doi.org/10.1016/j.rse.2019.111479, 2020.

ESA: Land Cover CCI Product User Guide Version 2. Tech. Rep., maps.elie.ucl.ac.be/CCI/viewer/download/ESACCI-LC-Ph2-PUGv2_2.0.pdf, last access: February 12, 2025, 2017.